Letter

Anomalous Floquet Anderson insulator in a continuously driven optical lattice

Arijit Dutta [1], Efe Sen [1], Jun-Hui Zheng [2,3], Monika Aidelsburger [4,5,6] and Walter Hofstetter [1]

[1] *Goethe-Universität, Institut für Theoretische Physik, 60438 Frankfurt am Main, Germany*
[2] *Shaanxi Key Laboratory for Theoretical Physics Frontiers, Institute of Modern Physics, Northwest University, Xi'an 710127, China*
[3] *Peng Huanwu Center for Fundamental Theory, Xi'an 710127, China*
[4] *Max-Planck-Institut für Quantenoptik, Hans-Kopfermann-Strasse 1, 85748 Garching, Germany*
[5] *Fakultät für Physik, Ludwig-Maximilians-Universität, Schellingstrasse 4, 80799 München, Germany*
[6] *Munich Center for Quantum Science and Technology (MCQST), Schellingstraße 4, 80799 München, Germany*

(Received 28 December 2023; accepted 4 February 2024; published 25 March 2024)

The anomalous Floquet Anderson insulator (AFAI) has been theoretically predicted in stepwise periodically driven models, but its stability under more general driving protocols has not been determined. We show that adding disorder to the anomalous Floquet topological insulator realized with a continuous driving protocol in the experiment by Wintersperger *et al.* [Nat. Phys. **16**, 1058 (2020)], supports an AFAI phase, where, for a range of disorder strengths, all the time averaged bulk states become localized, while the pumped charge in a Laughlin pump setup remains quantized.

DOI: 10.1103/PhysRevB.109.L121114

Introduction. Periodically driven quantum systems have led to interesting phenomena in different experimental platforms [1–6] and are particularly useful in the realization of nontrivial effective equilibrium states [6–10]. The realization of topological models such as the Hofstadter [11–13], the Haldane [14–18] and the interacting Rice-Mele model [19–21] have been reported in ultracold atom and photonic systems [22–26]. Most of these employ the high driving-frequency limit, where multiphoton absorption processes are suppressed [2]. However, when the driving frequency becomes comparable to the other energy scales of the driven system, novel types of steady-state phases appear, which have no counterpart in equilibrium systems [1,27,28]. New features in the band structure show up due to multiple-photon processes between neighboring bands which can survive even with weak two-body interactions [29]. The anomalous Floquet topological insulator (AFTI), with a novel bulk-boundary correspondence was first theoretically predicted [27,28] with a step-driving protocol, and realized in photonic systems [25,26]. The crucial aspect for stabilizing the AFTI phase is the breaking of time-reversal symmetry by circular driving, and hence, the discrete nature of the drive does not play a major role. The AFTI system was realized in an ultracold atomic hexagonal lattice, with a continuous circular driving protocol, by modulating the amplitudes of three laser beams out of phase [16–18].

Adding disorder to the AFTI phase can lead to a remarkable new phase, the anomalous Floquet Anderson insulator (AFAI), at an intermediate disorder strength which is comparable to the driving frequency. The phase is characterized by the complete localization of all bulk states together with the existence of robust edge states at all energies. This leads to quantized pumping of charge, even when all the bulk states are localized, which is impossible in equilibrium systems. In spite of theoretical predictions in idealized models [30,31], it has not been experimentally realized. The realization of this phase in ultracold atoms will, additionally, allow us to study the interplay with two-body interactions in a controlled way.

Our work provides numerical evidence that it is indeed possible to stabilize the AFAI phase in the experimentally accessible parameter regimes. However, its indicators are strongly system size dependent. This is because complete localization of bulk states for two-dimensional systems can only be realized for very large system sizes. By considering a Laughlin pump setup we show that the pumped charge over one period of the threaded flux remains quantized even when *all* bulk states become localized. We work with the continuous driving protocol implemented on a honeycomb lattice as realized in Refs. [16,17], and add on-site disorder to it. The honeycomb lattice has a two-sublattice structure which we denote by labels A and B [Fig. 1(a)]. The real-space Hamiltonian is ($\hbar = 1$)

$$H(t) = \sum_{\boldsymbol{i}} \sum_{\gamma=1}^{3} \left(J_\gamma(t) c_{\boldsymbol{i}}^\dagger c_{\boldsymbol{i}+\boldsymbol{\beta}_{\boldsymbol{i}\gamma}} + \text{H.c.}\right) + \sum_{\boldsymbol{i}} V_{\boldsymbol{i}} c_{\boldsymbol{i}}^\dagger c_{\boldsymbol{i}}, \quad (1)$$

where $c_{\boldsymbol{i}}^\dagger (c_{\boldsymbol{i}})$ creates (annihilates) a spinless fermion at site $\boldsymbol{i}$, $J_\gamma(t) = J \exp[F \cos(\Omega t + \phi_\gamma)]$, with $\phi_\gamma = \frac{2\pi}{3}(\gamma - 1)$, are the hoppings across three nearest-neighbor bonds $\boldsymbol{\beta}_{\boldsymbol{i}\gamma}$ at each site $\boldsymbol{i}$. If the vector $\boldsymbol{i}$ points to a site in the $A\,(B)$ sublattice then $\boldsymbol{\beta}_{\boldsymbol{i}\gamma} = +(-)\boldsymbol{\delta}_\gamma$ (for $\gamma = 1, 2, 3$), where $\boldsymbol{\delta}_1 \equiv (0, a)$, $\boldsymbol{\delta}_2 \equiv (-\sqrt{3}a/2, -a/2)$, $\boldsymbol{\delta}_3 \equiv (\sqrt{3}a/2, -a/2)$ [Fig. 1(*a*)], a is the lattice constant, J is the bare hopping amplitude, Ω is the driving frequency and F is a dimensionless parameter which controls the width of the bulk bands [32]. $V_{\boldsymbol{i}}$ is an on-site disorder potential which is sampled from a uniform distribution of width W and zero mean.

According to Floquet's theorem, such a time-periodic Hamiltonian admits stationary solutions, called *Floquet states*, of the form $|\psi_\alpha(t)\rangle = \exp(-i\varepsilon_\alpha t)|u_\alpha(t)\rangle$, where ε_α is the time-independent *quasienergy* and

 ©2024 American Physical Society

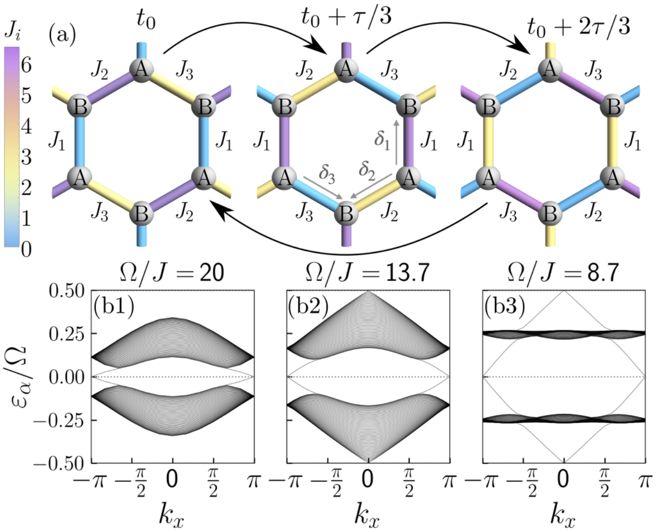

FIG. 1. (a) The driving protocol on the honeycomb lattice, where the hopping amplitudes at each step are represented by false color. Quasienergy spectrum at characterisic Ω/J values, (b1) 20, (b2) 13.7, and (b3) 8.7 for a zigzag semi-infinite strip with 48 unit cells and $F = 2$. (b1) denotes a CI regime where edge states corresponding to nonvanishing bulk Chern number appear in the 0 gap. As the driving frequency is lowered the π gap closes (b2) and reopens, leading to an AFTI regime (b3) having edge states in all gaps but vanishing Chern number of the bulk bands.

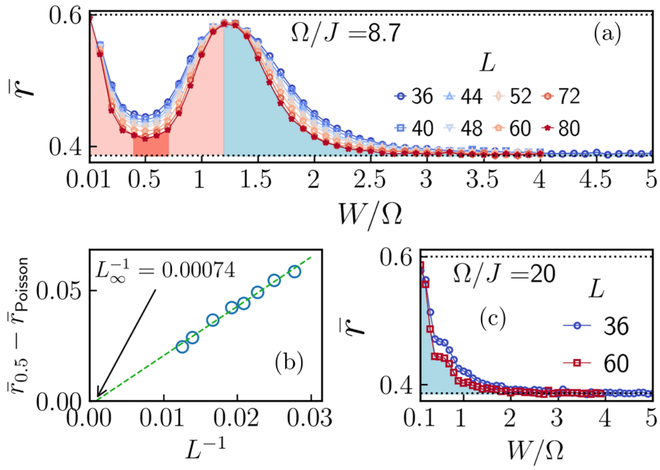

FIG. 2. (a) Variation of the average LSR ($\bar{r}$) with W/Ω at $\Omega/J = 8.7$. Level statistics in the delocalized regime for $W/\Omega \leqslant 0.01$ is characterized by $\bar{r} \approx \bar{r}_{\text{GUE}} \approx 0.6$, and for the Anderson localized regime for $W/\Omega \geqslant 3$ by $\bar{r} \approx \bar{r}_{\text{Poisson}} \approx 0.39$. $\bar{r}$ has a dip at $W/\Omega \approx 0.5$, where $\bar{r}$ approaches $\bar{r}_{\text{Poisson}}$ with increasing system size, and a peak at $W/\Omega \approx 1.2$. At the largest accessible size (80×80), the region marked in red has localized states at all quasienergies (Fig. 3) in the first FBZ, while the regions shown in orange and turquoise show intermediate behavior. The red region is expected to grow while the light red and turquiose regions are expected to shrink with increasing size, and ultimately vanish in the limit of infinite system size, leading to sharp localization-delocalization-localization transitions. (b) Behavior of $\bar{r}$ at $W/\Omega = 0.5$ ($\bar{r}_{0.5}$) with increasing linear dimension L of the system. The best fit (green) line indicates that $\bar{r}_{0.5}$ should approach $\bar{r}_{\text{Poisson}}$ for $L \gtrsim 10^3$. (c) $\bar{r}$ variation with W/Ω at $\Omega/J = 20$. The system goes from the delocalized Chern insulator phase for $W/\Omega < 0.1$ to a localized Anderson insulator phase for $W/\Omega \geqslant 2$ with an intermediate (blue) region which shrinks with increasing size.

$|u_\alpha(t)\rangle = |u_\alpha(t+\tau)\rangle$ is periodic with the time-period $\tau = 2\pi/\Omega$ of the drive. Hence, $|u_\alpha(t)\rangle$ can be expanded in its harmonics $|u_\alpha^{(n)}\rangle = \int_0^\tau (\mathrm{d}t/\tau)\exp(in\Omega t)|u_\alpha(t)\rangle$, where n is an integer. The Hamiltonian in Eq. (1) can be diagonalized by Fourier transformation [33] to obtain a time-independent eigenvalue problem for the Floquet harmonics $\sum_{j,m} \tilde{H}_{ij}^{(n,m)} u_{j\alpha}^{(m)} = \varepsilon_\alpha u_{i\alpha}^{(n)}$, where $\tilde{H}_{ij}^{(n,m)} = \frac{1}{\tau}\int_0^\tau \mathrm{d}t\, e^{i(n-m)\Omega t} H_{ij}(t) - m\Omega\delta_{nm}\delta_{ij}$ is the "Floquet Hamiltonian" [28], $H_{ij}(t)$ is the representation of $H(t)$ in a site-localized basis $\{|i\rangle\}$, and $u_{i\alpha}^{(m)} \equiv \langle i|u_\alpha^{(m)}\rangle$ is the wave function of the mth harmonic of $|u_\alpha(t)\rangle$ (m is an integer). Henceforth, the index α shall be restricted to the quasienergies in the first Floquet Brillouin zone (FBZ) $-\Omega/2 \leqslant \varepsilon_\alpha < \Omega/2$ [34].

Anomalous Floquet topological insulator (AFTI). We first consider a clean system. In Fig. 1, we plot the dispersion of a semi-infinite strip with zigzag edges for $\Omega/J = 20,\ 13.7,\ 8.7$, and $|m|, |n| \leqslant N = 9$. We define two gaps, the $0(\pi)$ gap having magnitude $\Delta_{0(\pi)}$, respectively, at the center and the edge of the FBZ for bulk states. For $\Omega/J = 20$, the system is a Chern insulator (CI). On decreasing Ω/J, Δ_π vanishes at $\Omega/J \approx 13.7$ and the system undergoes a transition from a CI phase to an AFTI phase, akin to that realized in the experiments [16,17]. The dispersion for a zigzag strip when Ω/J is tuned across the transition is shown in Fig. 1. In each FBZ, the Chern number of the upper (lower) band ($C^\pm$) is given by $C^\pm = \mp(\mathcal{W}_0 - \mathcal{W}_\pi)$, where $\mathcal{W}_{0(\pi)}$ is an integer topological invariant for the periodically driven bulk system, called the winding number, which counts the number of chiral edge modes within the gap at quasienergy $0(\Omega/2)$ when the system is defined on a semi-infinite strip. This justifies how the Chern number for all the bulk bands in the anomalous phase can be zero while it hosts robust chiral edge states [27,28].

Effect of disorder on the bulk. We focus on two characteristic driving frequencies, $\Omega/J = 20$ in the CI phase and $\Omega/J = 8.7$ in the AFTI phase, and study the effect of onsite disorder in the bulk. The degree of localization in a disordered system can be characterized by the *level spacing ratio* (LSR) r_α given by $r_\alpha = \min\{s_\alpha, s_{\alpha-1}\}/\max\{s_\alpha, s_{\alpha-1}\}$, where α labels the quasienergies within the first FBZ and $s_\alpha = \varepsilon_{\alpha+1} - \varepsilon_\alpha$ is the spacing between consecutive quasienergy levels. The disorder-averaged LSR distribution is given by $p(r) = \langle \sum_\alpha \delta(r - r_\alpha)\rangle$, where $\langle ..\rangle$ denotes disorder averaging. Results from random matrix theory suggest that $p(r)$ has a Poissonian form, characterized by the mean LSR ($\bar{r}$) approaching $\bar{r}_{\text{Poisson}} = 2\ln 2 - 1 \approx 0.39$, if all the states in the system are localized. On the other hand, $p(r)$ in a system without time-reversal invariance, in the thermodynamic limit, for extended states is given by a Wigner-Dyson form corresponding to the Gaussian unitary ensemble (GUE), which is characterized by $\bar{r}_{\text{GUE}} = 2\sqrt{3}/\pi - 1/2 \approx 0.60$ [30,35–37]. Figures 2(a) and 2(c) show the behavior of $\bar{r}$ as a function of disorder strength W/Ω for $\Omega/J = 8.7$ and 20, respectively. The two-peak structure for $\Omega/J = 8.7$, along with its size dependence, indicates the presence of a localized bulk phase

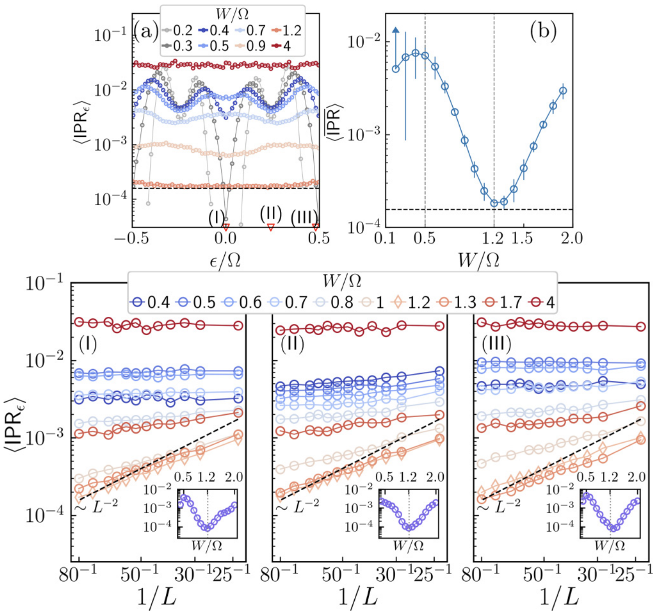

FIG. 3. (a) $\langle \mathrm{IPR}_\epsilon \rangle$ for different disorder strengths W/Ω for $L = 80$ at $\Omega/J = 8.7$. The vertical cuts at center (I), three-quarters (II) and edge (III) of the FBZ are selected and their size-dependence is shown in the bottom panel. (b) Behavior of $\langle \overline{\mathrm{IPR}} \rangle$, the ϵ average of $\langle \mathrm{IPR}_\epsilon \rangle$, with varying W/Ω. Error bars indicate the standard deviation. For $W/\Omega = 0.2$ only one-sided error is shown since the lower bound does not fit the plot range. The horizontal dashed black lines in both (a) and (b) correspond to 80^{-2}, which sets the reference level for L^{-2} scaling of $\langle \mathrm{IPR}_\epsilon \rangle$. Bottom: Log-log plots of $\langle \mathrm{IPR}_\epsilon \rangle$ as a function of L for states at the selected values of ε/Ω indicated by the red triangles in (a). For $0.4 \lesssim W/\Omega \lesssim 0.7$ the system shows complete localization marked by a size independent IPR for large L at all quasienergies ϵ. For $W/\Omega \approx 1.2$ the system becomes delocalised for large L, as inferred from the slope of the corresponding trace. It should be compared with the black dashed line which corresponds to L^{-2} scaling and represents the ideal delocalization limit in 2d. The insets track the behavior of $\langle \mathrm{IPR}_\varepsilon \rangle$ versus W/Ω for $L = 80$. The dip occurs around $W/\Omega = 1.2$ for the three energy slices.

around $W/\Omega \approx 0.5$, which is different from the Anderson insulator (AI) phase realized for $W/\Omega \geqslant 3$. Moreover, the transition from this novel localized phase, which we call the anomalous localized phase, to the AI phase involves a "critical" point [30], at $W/\Omega \approx 1.2$, where $\bar{r}$ attains a maximum value [38].

To investigate the localization properties of the anomalous localized phase in more detail, we consider the *inverse participation ratio* (IPR) for the time-averaged state $|u_\alpha^{(0)}\rangle$, defined, for each disorder realization, as $\mathrm{IPR}_\epsilon \equiv \sum_{i,\alpha} |\langle i|u_\alpha^{(0)}\rangle|^4 \delta(\epsilon - \varepsilon_\alpha)$, where $|i\rangle$ is the site basis state [39]. Figure 3(a) shows the disorder averaged IPR, $\langle \mathrm{IPR}_\epsilon \rangle$ for ϵ in the first FBZ, for different disorder strengths W/Ω. For $W/\Omega < 0.3$, the spectrum has a gap at $\epsilon/\Omega = 0$ and ± 0.5, even for the largest system size which could be accessed (80×80). For $W/\Omega \approx 0.3$, the spectrum becomes gapless for large L, but has a gap at lower L values, while for $W \geqslant 0.4$ the spectrum remains gapless for all the accessed L values. In order to understand the overall behavior of $\langle \mathrm{IPR}_\epsilon \rangle$ with changing W, we show its mean over ϵ, $\langle \overline{\mathrm{IPR}} \rangle$, along with the corresponding standard deviation in

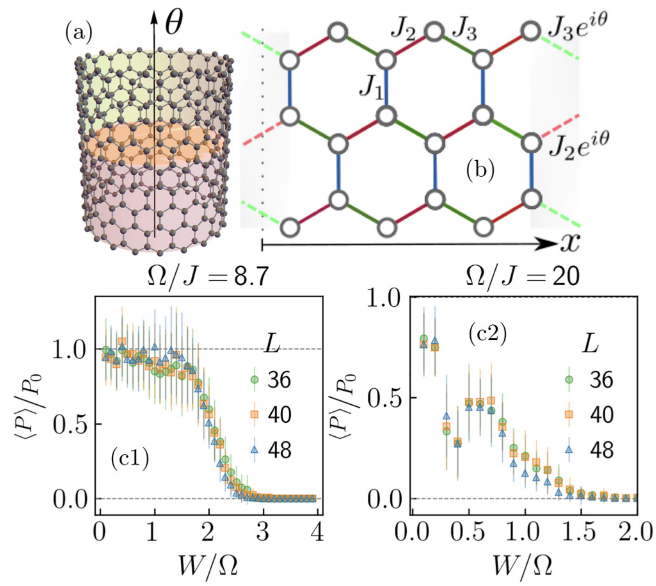

FIG. 4. (a) The Laughlin pump setup where a flux θ is threaded through a cylindrical system. (b) The gauge choice in which additional phases $e^{i\theta}$ are acquired by the hopping amplitudes across the bonds which intersect the $x = 0$ (dotted) line. Bottom: Variation of the disorder normalized average pumped charge $\langle P \rangle / P_0$, with disorder strength W/Ω for $\Omega/J = 8.7$ (c1) and 20 (c2). For $0.1 \leqslant W/\Omega \lesssim 1.2$, in the anomalous phase (c1) $\langle P \rangle / P_0$ remains quantized to the value 1 (within error bars), and decays to zero with increasing disorder strength. In the CI phase (c2), $\langle P \rangle / P_0$ is reduced below 1 even for the lowest disorder strength considered, and decays to zero with increasing disorder. The transitions become sharper with increasing linear dimension L.

Fig. 3(b). As W/Ω increases, $\langle \overline{\mathrm{IPR}} \rangle$ attains its maximum value near $W/\Omega = 0.5$, indicating a maximally localized state on average, and minimum value near $W/\Omega = 1.2$, indicating that on average, a maximum number of states are delocalized.

To further support these observations, we show the size dependence of $\langle \mathrm{IPR}_\epsilon \rangle$ at three characteristic quasienergies chosen at the center (I), three-quarters (II) and edge (III) of the first FBZ in the bottom panel of Fig. 3. These points are indicated by red triangles in Fig. 3(a). We find that for $0.4 \leqslant W/\Omega \leqslant 0.7$, $\langle \mathrm{IPR}_\epsilon \rangle$ remains L independent for $L \geqslant 60$, across all the three ϵ slices. Hence, we expect the bulk states at all quasienergies to be localized for this range of W values. Even for lower L values $\langle \mathrm{IPR}_\epsilon \rangle$ shows almost no scaling at the center and edge of the first FBZ for these values of W/Ω, but shows scaling behavior for a quasienergy in between them [slice (II)]. Furthermore, at $W/\Omega \approx 1.2$ we find the emergence of L^{-2} scaling for large L, at all the three ϵ slices, even though the disorder strength is even larger than the bandwidth of the clean system. This confirms the presence of an additional localized phase around $W/\Omega = 0.5$ and a localization-delocalization transition around $W/\Omega = 1.2$, as indicated by the LSR.

Charge pumping. The topological properties of the phases can by evaluated by setting up a Laughlin charge pump, where a flux θ is threaded through the system in a cylindrical geometry [40,41], as shown in Fig. 4(a). Assuming that the zigzag edge of the cylinder is oriented along the x-direction, we choose a gauge such that the nearest-neighbor hopping elements across the bonds which intersect the line $x = 0$ acquire an additional phase $\exp(\pm i\theta)$ [30] for hopping to the right (left) [Fig. 4(b)]. The total occupancies in the upper ($\mathcal{U}$) and lower ($\mathcal{L}$) halves of the cylinder are given by $Q_{\mathcal{U}(\mathcal{L})}(\theta) = \sum_{i\in\mathcal{U}(\mathcal{L})} Q_i$, where Q_i is the occupancy of the site at position $\boldsymbol{i}$. The difference between the total particle numbers accumulated in the upper and lower halves of the cylinder is $\delta Q(\theta) = Q_{\mathcal{U}}(\theta) - Q_{\mathcal{L}}(\theta)$ and $P \equiv (\max\{\delta Q(\theta)\} - \min\{\delta Q(\theta)\})/2$ is the *pumped charge* in one period of the threaded flux θ. In a topologically nontrivial phase, the flux threading is accompanied by a discontinuity of δQ as θ is varied between $[0, 2\pi]$ [41]. The site occupancies Q_i can be expressed in terms of the lesser Floquet Green's function $G^<$ [33,41–43]

$$Q_i = \sum_{n=\frac{-N}{2}}^{\frac{N}{2}} \int_{-\Omega/2}^{\Omega/2} \frac{d\omega}{2\pi} \lim_{\Gamma\to 0^+} \mathrm{Im}[G^<_{i,n;i,n}(\omega;\theta)]$$
$$= \sum_\alpha \left(\sum_n \left|u^{(n)}_{i\alpha}\right|^2\right)\left(\sum_{l,p} f(\varepsilon_\alpha + p\Omega)\left|u^{(p)}_{l\alpha}\right|^2\right), \quad (2)$$

where $f(\omega) \equiv (1 + \exp(\omega/T))^{-1}$, and n and p are integers [44]. We use Q_i to calculate the disorder-averaged steady-state pumped charge $\langle P\rangle$, normalized by its reference value P_0 in the clean system, by tracking the θ dependence of δQ for every disorder realization. $\langle P\rangle/P_0$ has been plotted in Fig. 4 ($c1$) for $\Omega/J = 8.7$ in the anomalous localized phase and in Fig. 4 ($c2$) for $\Omega/J = 20$ in the CI phase. We find that $\langle P\rangle/P_0$ remains quantized in the anomalous phase for $W/\Omega < 1.2$, while it decreases rapidly with increasing W/Ω in the CI phase [45]. This means the phase at $\Omega/J = 8.7$ supports quantized charge pumping through the edge states while its time-averaged bulk states remain completely localized for $0.4 \leqslant W/\Omega \leqslant 0.7$. This is the signature of the AFAI phase, as discussed in Ref. [30], which supports one chiral edge mode at each edge of the cylinder, and the two edge modes have opposite chiralities.

Discussion. When all the bulk states are localized then the Chern number at any quasienergy must be zero. However, we find that two chiral edge states, each localized at one of edges of the system defined on a cylinder coexist with the localized bulk states [33]. The quasienergies of chiral edge states have a nontrivial flow under flux threading, which gives rise to a quantized pumped charge, as was previously observed in Ref. [30]. The localized bulk states do not flow under threading of flux and hence do not contribute to the charge pumping. It was also shown in Ref. [30] that if one of the edge modes is fully occupied, while the other remains unoccupied, then the net charge flowing across any bond on the occupied edge, per unit time remains quantized, and is equal to the winding number in the bulk when the system has been driven over many cycles. Here we show that the net charge pumped from the bulk to the edges when one quantum of flux is threaded through the cylinder also remains quantized.

Tuning F away from $F = 2$, for $\Omega/J = 8.7$, increases the dispersion of the bulk bands which has a destabilizing effect on the AFAI phase. We find that the AFAI is stable between $1.9 \leqslant F \leqslant 2.1$ [33]. Topological edge states have been observed in ultracold atoms by creating a programmable repulsive potential and releasing a localized Bose-Einstein condensate near the edge using an optical tweezer. Subsequently, in the clean system, the wave packet propagates along the potential boundary, following its curvature, which is a characteristic for chiral edge states [17]. Such chiral motion at the potential boundary should also be observable in the AFAI, while, in contrast, once the repulsive potential is switched off the initial wave packet should remain localized [46].

Conclusion. We have studied localization properties and charge pumping in a disordered, circularly driven honeycomb lattice with a continuous driving protocol realized in the experiments [16,17]. Within the scope of finite size numerics, we found that a new phase emerges at intermediate disorder strength, in which the time-averaged bulk states are fully localized while the system supports quantized charge pumping via edge states, when the system has been evolved over many driving cycles. This is the AFAI phase, previously predicted in a simplified model [30] which is difficult to realize with ultracold atoms. We also show that the quantized charge pumping in the AFAI phase remains robust at intermediate disorder strength, in contrast to the CI phase. Our approach will also allow us to study the interplay of on-site interactions and strong disorder in the periodically driven system, which can lead to discovery of new phases in hitherto unexplored parameter regimes using Floquet-dynamical mean-field theory [29,41].

Acknowledgments. This work was supported by the Deutsche Forschungsgemeinschaft (DFG, German Research Foundation) under Project No. 277974659 via Research Unit FOR 2414. J.-H.Z. acknowledges support from the NSFC under Grants No.12247103 and No.12175180, Shaanxi Fundamental Science Research Project for Mathematics and Physics under Grants No. 22JSQ041 and No. 22JSZ005, and the Youth Innovation Team of Shannxi Universities. M.A. also acknowledges support from the Deutsche Forschungsgemeinschaft (DFG) under Germany's Excellence Strategy - EXC-2111 - 390814868. A.D. thanks Y. Xu for helpful discussions. The authors gratefully acknowledge the Gauss Centre for Supercomputing e.V. [47] for funding this project by providing computing time through the John von Neumann Institute for Computing (NIC) on the GCS Supercomputer JUWELS at Jülich Supercomputing Centre (JSC). Calculations for this research were also performed on the Goethe-NHR high performance computing cluster. The cluster is managed by the Center for Scientific Computing (CSC) of the Goethe University Frankfurt.

[1] M. S. Rudner and N. H. Lindner, Nat. Rev. Phys. **2**, 229 (2020).
[2] A. Eckardt and E. Anisimovas, New J. Phys. **17**, 093039 (2015).
[3] M. Holthaus, J. Phys. B **49**, 013001 (2016).
[4] A. Eckardt, Rev. Mod. Phys. **89**, 011004 (2017).
[5] C. Weitenberg and J. Simonet, Nat. Phys. **17**, 1342 (2021).
[6] W. Hofstetter and T. Qin, J. Phys. B **51**, 082001 (2018).

[7] M. Aidelsburger, S. Nascimbene, and N. Goldman, C. R. Phys. **19**, 394 (2018).
[8] R. Citro and M. Aidelsburger, Nat. Rev. Phys. **5**, 87 (2023).
[9] N. R. Cooper, J. Dalibard, and I. B. Spielman, Rev. Mod. Phys. **91**, 015005 (2019).
[10] T. Ozawa, H. M. Price, A. Amo, N. Goldman, M. Hafezi, L. Lu, M. C. Rechtsman, D. Schuster, J. Simon, O. Zilberberg, and I. Carusotto, Rev. Mod. Phys. **91**, 015006 (2019).
[11] M. Aidelsburger, M. Atala, M. Lohse, J. T. Barreiro, B. Paredes, and I. Bloch, Phys. Rev. Lett. **111**, 185301 (2013).
[12] H. Miyake, G. A. Siviloglou, C. J. Kennedy, W. C. Burton, and W. Ketterle, Phys. Rev. Lett. **111**, 185302 (2013).
[13] M. Aidelsburger, M. Lohse, C. Schweizer, M. Atala, J. T. Barreiro, S. Nascimbne, N. R. Cooper, I. Bloch, and N. Goldman, Nat. Phys. **11**, 162 (2015).
[14] G. Jotzu, M. Messer, R. Desbuquois, M. Lebrat, T. Uehlinger, D. Greif, and T. Esslinger, Nature (London) **515**, 237 (2014).
[15] N. Fläschner, B. S. Rem, M. Tarnowski, D. Vogel, D. S. Lühmann, K. Sengstock, and C. Weitenberg, Science **352**, 1091 (2016).
[16] K. Wintersperger, C. Braun, F. N. Ünal, A. Eckardt, M. D. Liberto, N. Goldman, I. Bloch, and M. Aidelsburger, Nat. Phys. **16**, 1058 (2020).
[17] C. Braun, R. Saint-Jalm, A. Hesse, J. Arceri, I. Bloch, and M. Aidelsburger, arXiv:2304.01980.
[18] J.-H. Zheng, A. Dutta, M. Aidelsburger, and W. Hofstetter, arXiv:2309.07035.
[19] M. Lohse, C. Schweizer, O. Zilberberg, M. Aidelsburger, and I. Bloch, Nat. Phys **12**, 350 (2016).
[20] S. Nakajima, T. Tomita, S. Taie, T. Ichinose, H. Ozawa, L. Wang, M. Troyer, and Y. Takahashi, Nat. Phys **12**, 296 (2016).
[21] A. S. Walter, Z. Zhu, M. Gächter *et al.*, Nat. Phys. **19**, 1471 (2023).
[22] M. Rechtsman, J. M. Zeuner, Y. Plotnik, Y. Lumer, D. Podolsky, F. Dreisow, S. Nolte, M. Segev, and A. Szameit, Nature (London) **496**, 196 (2013).
[23] M. Hafezi, S. Mittal, J. Fan, A. Migdall, and J. M. Taylor, Nat. Photonics **7**, 1001 (2013).
[24] S. Mittal, V. V. Orre, D. Leykam, Y. D. Chong, and M. Hafezi, Phys. Rev. Lett. **123**, 043201 (2019).
[25] L. J. Maczewsky, J. M. Zeuner, S. Nolte, and A. Szameit, Nat. Commun. **8**, 13756 (2017).
[26] S. Mukherjee, A. Spracklen, M. Valiente, E. Andersson, P. Öhberg, N. Goldman, and R. R. Thomson, Nat. Commun. **8**, 13918 (2017).
[27] T. Kitagawa, E. Berg, M. Rudner, and E. Demler, Phys. Rev. B **82**, 235114 (2010).
[28] M. S. Rudner, N. H. Lindner, E. Berg, and M. Levin, Phys. Rev. X **3**, 031005 (2013).
[29] T. Qin and W. Hofstetter, Phys. Rev. B **96**, 075134 (2017).
[30] P. Titum, E. Berg, M. S. Rudner, G. Refael, and N. H. Lindner, Phys. Rev. X **6**, 021013 (2016).
[31] A. Kundu, M. Rudner, E. Berg, and N. H. Lindner, Phys. Rev. B **101**, 041403(R) (2020).
[32] Henceforth, we set $a = 1$, $J = 1$ and $F = 2$.
[33] See Supplemental Material at http://link.aps.org/supplemental/10.1103/PhysRevB.109.L121114 for Floquet theory and Floquet Green's functions, a derivation of the expression for pumped charge, a demonstration of spectral flow in the disordered system, and a discussion of the effect of band dispersion on the localization properties of the bulk.
[34] It can be easily verified that for two integers n and p, if $u_{i\alpha}^{(n)}$ satisfies $\sum_{j,m}\tilde{H}_{ij}^{(n,m)}u_{j\alpha}^{(m)} = \varepsilon_\alpha u_{i\alpha}^{(n)}$ with the quasienergy ε_α, then $u_{i\alpha}^{(n+p)}$ also satisfies the same eigenvalue problem with quasienergy $\varepsilon_\alpha + p\Omega$.
[35] Y. Y. Atas, E. Bogomolny, O. Giraud, and G. Roux, Phys. Rev. Lett. **110**, 084101 (2013).
[36] V. Oganesyan and D. A. Huse, Phys. Rev. B **75**, 155111 (2007).
[37] T. Guhr, A. Müller-Groeling, H. A. Weidenmüller, Phys. Rep. **299**, 189 (1998).
[38] In the thermodynamic limit, we expect the transition from the anomalous localized phase to the AI phase to be "infinitely sharp" which is supported by the finite size scaling shown in Fig. 2(b).
[39] IPR_ϵ scales as L^{-2} for extended states in two dimensions, where L is the linear dimension. For localized states it becomes independent of system size, for sufficiently large L.
[40] R. B. Laughlin, Phys. Rev. B **23**, 5632(R) (1981).
[41] T. Qin, A. Schnell, K. Sengstock, C. Weitenberg, A. Eckardt, and W. Hofstetter, Phys. Rev. A **98**, 033601 (2018).
[42] H. Aoki, N. Tsuji, M. Eckstein, M. Kollar, T. Oka, and P. Werner, Rev. Mod. Phys. **86**, 779 (2014).
[43] T. Qin and W. Hofstetter, Phys. Rev. B **97**, 125115 (2018).
[44] In order to specify an initial state we have introduced a bath at temperature T which is quadratically coupled to the system with a coupling strength Γ [33,43]. However, the experimentally prepared ultracold atomic systems are essentially isolated, so we take the limit $\Gamma \to 0$ and set $T = 0.01$ in Eq. (2).
[45] For different disorder realizations, the discontinuities appear at different θ values. In the numerical implementation, working with a fixed θ grid makes it impossible to capture the discontinuity for all disorder realizations. This further smears out the transition from the AFAI to the AI phase, and from the CI to AI phase.
[46] For weak disorder, when the system is not in the AFAI phase, sufficiently high energy wave packets, within the first FBZ, will not remain localized, while for strong disorder when the system is in the AI phase, there should be no chiral motion at the edge.
[47] www.gauss-centre.eu.